1   **Ozone Production and Its Sensitivity to NO_x and VOCs: Results from the DISCOVER-AQ**

2   **Field Experiment, Houston 2013**

3   Gina M. Mazzuca[1], Xinrong Ren[1,2,*], Christopher P. Loughner[2,3], Mark Estes[5], James H.

4   Crawford[6], Kenneth E. Pickering[1,4], Andrew J. Weinheimer[7], and Russell R. Dickerson[1]

5   [1]Department of Atmospheric and Oceanic Science, University of Maryland, College Park, MD

6   20742, USA

7   [2]Air Resources Laboratory, National Oceanic and Atmospheric Administration, College Park,

8   MD 20740, USA

9   [3]Earth System Science Interdisciplinary Center, University of Maryland, College Park, MD

10   20740, USA

11   [4]NASA Goddard Space Flight Center, Greenbelt, MD 20771, USA

12   [5]Texas Commission on Environmental Quality, Austin, TX 78711, USA

13   [6]NASA Langley Research Center, Hampton, VA 23681, USA

14   [7] National Center for Atmospheric Research, Boulder, CO 80307, USA

15

16

17   *Correspondence to: X. Ren (ren@umd.edu)

18

19   **Abstract** An observation-constrained box model based on the Carbon Bond mechanism, Version

20   5 (CB05), was used to study photochemical processes along the NASA P-3B flight track and

21   spirals over eight surface sites during the September 2013 Houston, Texas deployment of the

22   NASA DISCOVER-AQ campaign. Data from this campaign provided an opportunity to examine

23   and improve our understanding of atmospheric photochemical oxidation processes related to the

24   formation of secondary air pollutants such as ozone (O_3). O_3 production and its sensitivity to

25   NO_x and VOCs were calculated at different locations and times of day. Ozone production

26   efficiency (OPE), defined as the ratio of the ozone production rate to the NO_x oxidation rate, was

27   calculated using the observations and the simulation results of the box and Community

28   Multiscale Air Quality (CMAQ) models. Correlations of these results with other parameters,

29   such as radical sources and NO_x mixing ratio, were also evaluated. It was generally found that O_3

30   production tends to be more VOC sensitive in the morning along with high ozone production

31   rates, suggesting that control of VOCs may be an effective way to control O_3 in Houston. In the

32   afternoon, O_3 production was found to be mainly NO_x sensitive with some exceptions. O_3

33   production near major emissions sources such as Deer Park was mostly VOC sensitive for the

34   entire day, other urban areas near Moody Tower and Channelview were VOC sensitive or in the

35   transition regime, and areas farther from downtown Houston such as Smith Point and Conroe

36   were mostly NO_x sensitive for the entire day. It was also found that the control of NO_x emissions

37   has reduced O_3 concentrations over Houston, but has led to larger OPE values. The results from

38   this work strengthen our understanding of O_3 production; they indicate that controlling NO_x

39   emissions will provide air quality benefits over the greater Houston metropolitan area in the long

40   run, but in selected areas controlling VOC emissions will also be beneficial.

41

42   **Keywords** Ozone production; Ozone Production Efficiency; Houston; DISCOVER-AQ

43

44   **1. Introduction**

45   Understanding the non-linear relationship between ozone production and its precursors is

46   critical for the development of an effective ozone (O_3) control strategy. Despite great efforts

47   undertaken in the past decades to address the problem of high ozone concentrations, our

48   understanding of the key precursors that control tropospheric ozone production remains

49   incomplete and uncertain [Molina and Molina, 2004; Xue et al., 2013]. Atmospheric ozone

50   levels are determined by emissions of ozone precursors, atmospheric photochemistry, and

51   transport [Jacob, 1999; Xue et al., 2013]. A major challenge in regulating ozone pollution lies in

52   comprehending its complex and non-linear chemistry with respect to ozone precursors, i.e.,

53   nitrogen oxides (NO_x) and volatile organic compounds (VOCs) that varies with time and location

54   (Figure 1). Understanding the non-linear relationship between ozone production and its

55   precursors is critical for the development of an effective ozone control strategy.

56   Sensitivity of ozone production to NO_x and VOCs represents a major uncertainty for

57   oxidant photochemistry in urban areas [Sillman et al., 1995; 2003]. In urban environments,

58   ozone is formed through photochemical processes when its precursors NO_x and VOCs are

59   emitted into the atmosphere from many sources. Depending on physical and chemical conditions,

60   the production of ozone can be either NO_x-sensitive or VOC-sensitive due to the complexity of

61   these photochemical processes. Therefore, effective ozone control strategies rely heavily on the

62   accurate understanding of how ozone responds to reduction of NO_x and VOC emissions, usually

63   simulated by photochemical air quality models [e.g., Sillman et al., 2003; Lei et al., 2004; Mallet

64   and Sportisse, 2005; Li et al, 2007; Chen et al., 2010; Tang et al., 2010; Xue et al., 2013;

65   Goldberg et al., 2016]. However, those model-based studies have inputs or parameters subject to

66   large uncertainties that can affect not only the simulated levels of ozone but also the ozone

67   dependence on its precursors.

68   There are some observation-based studies of ozone production and its relationships with

69   NO_x and VOCs [e.g., Thielmann et al., 2002; Zaveri et al., 2003; Ryerson et al., 2003; Griffin et

70   al., 2003; Kleinman et al., 2005a; Neuman et al., 2009; Mao et al., 2010; Ren et al., 2013]. Using

71   in-situ aircraft observations, Kleinman et al. [2005a] studied five U.S. cities and found that ozone

72   production rates vary from nearly zero to 155 ppb hr^{-1} with differences depending on precursor

73   concentrations NO_x, and VOCs. They also found that in Houston, NO_x and light olefins are co-

74   emitted from petrochemical facilities leading to the highest ozone production of the five cities

75   [Kleinman et al., 2005a]. Using the data collected at a single surface location during the Study of

76   Houston Atmospheric Radical Precursors (SHARP) in spring 2009, the temporal variation of O_3

77   production was observed: VOC-sensitive in the early morning and NO_x-sensitive for most of the

78   afternoon [Ren et al., 2013]. This is similar to the behavior observed in two previous

79   summertime studies in Houston: the Texas Air Quality Study in 2000 (TexAQS 2000) and the

80   TexAQS II Radical and Aerosol Measurement Project in 2006 (TRAMP 2006) [Mao et al., 2010;

81   Chen et al., 2010]. In a more recent study using measurements in four cities in China, ozone

82   production was found to be in a VOC-sensitive regime in both Shanghai and Guangzhou, but in a

83   mixed regime in Lanzhou [Xue et al., 2013]. In the work presented here, we provide

84   investigations of spatial and temporal variations of ozone production and its sensitivity to NOx

85   and VOCs to provide a scientific basis to develop a non-uniform emission reduction strategy for

86   O_3 pollution control in urban and suburban areas such as the greater Houston metropolitan area.

87   This work utilized observations made during the Deriving Information on Surface

88   Conditions from COlumn and VERtically Resolved Observations Relevant to Air Quality

89   (DISCOVER-AQ) campaign in Houston in September 2013. This field campaign is unique due

90   to the comprehensive air sampling performed over a large spatial (urban and suburban areas in

91   and around Houston) and temporal (entire month of September 2013) range. Measurements were

92   collected from various platforms including the National Aeronautics and Space Administration

93   (NASA) P-3B and B-200 aircraft, ground surface sites, and mobile laboratories. Eight surface

94 monitoring stations (Smith Point, Galveston, Manvel Croix, Deer Park, Channelview, Conroe,

95 West Houston, and Moody Tower) were selected where the P-3B conducted vertical spirals

96 (Figure 2) [DISCOVER-AQ whitepaper].

97

98 **2. Methods**

99 **2.1 Ozone production Scenarios and Sensitivity**

100   During the day, the photochemical O_3 production rate is essentially the production rate of

101 NO_2 molecules from HO_2 + NO and RO_2 + NO reactions [Finlayson-Pitts and Pitts, 2000]. The

102 net instantaneous photochemical O_3 production rate, $P(O_3)$, can be written approximately as the

103 following equation:

104
$$P(O_3) = k_{HO_2+NO}[HO_2][NO] + \sum k_{RO_{2i}+NO}[RO_{2i}][NO] - k_{OH+NO_2+M}[OH][NO_2][M] - P(RONO_2)$$
$$- k_{HO_2+O_3}[HO_2][O_3] - k_{OH+O_3}[OH][O_3] - k_{O(^1D)+H_2O}[O(^1D)][H_2O] - L(O_3 + alkenes) \tag{1}$$

105 where, *k term*s are the reaction rate coefficients; RO_{2i} is the individual organic peroxy radicals.

106 The negative terms in Eq. (1) correspond to the reaction of OH and NO_2 to form nitric acid, the

107 formation of organic nitrates, $P(RONO_2)$, the reactions of OH and HO_2 with O_3, the photolysis of

108 O_3 followed by the reaction of $O(^1D)$ with H_2O, and O_3 reactions with alkenes. Ozone is

109 additionally destroyed by dry deposition.

110   The dependence of O_3 production on NO_x and VOCs can be categorized into two typical

111 scenarios: NO_x sensitive and VOC sensitive. The method proposed by Kleinman [2005b] was

112 used to evaluate the O_3 production sensitivity using the ratio of L_N/Q, where L_N is the radical

113 loss via the reactions with NO_x and Q is the total primary radical production. Because the radical

114 production rate is approximately equal to the radical loss rate, this L_N/Q ratio represents the

115 fraction of radical loss due to NO_x. It was found that when L_N/Q is significantly less than 0.5, the

116 atmosphere is in a NO_x-sensitive regime, and when L_N/Q is significantly greater than 0.5, the

117 atmosphere is in a more VOC-sensitive regime [Kleinman et al., 2001; Kleinman, 2005b]. Note

118 that the contribution of organic nitrates impacts the cut-off value for L_N/Q to determine the ozone

119 production sensitivity to NO_x or VOCs and this value may vary slightly around 0.5 in different

120 environments [Kleinman, 2005b].

121

122

123

124 **2.2 Box Model Simulations**

125   An observation-constrained box model with the Carbon Bond Mechanism Version 2005

126 (CB05) was used to simulate the oxidation processes in Houston during DISCOVER-AQ.

127 Measurements made on the P-3B were used as input to constrain the box model. From the box

128 model results, the ozone production rate and its sensitivity to NO_x and VOCs were calculated

129 allowing us to calculate ozone production efficiency at different locations and at different times

130 of day.

131   CB05 is a well-known chemical mechanism that has been actively used in research and

132 regulatory applications [Yarwood et al., 2005]. Organic species are lumped according to the

133 carbon bond approach, that is, bond type, e.g., carbon single bond and double bond. Reactions

134 are aggregated based on the similarity of carbon bond structure so that fewer surrogate species

135 are needed in the model. Some organics (e.g., organic nitrates and aromatics) are lumped. The

136 lifetime of alkyl nitrates is too long in CB05 and has been corrected in CB6r2 [Canty et al.,

137 2015], but this should have minimal impact on our findings because the model is constrained to

138 observations as indicated below.

139   The box model was run using measurements, including long-lived inorganic and organic

140 compounds and meteorological parameters (temperature, pressure, humidity, and photolysis

141 frequencies), from the NASA P-3B. One-minute archived data were used as model input

142 (available at http://www-air.larc.nasa.gov/missions/discover-aq/discover-aq.html). The model

143 ran for 24 hours for each data point to allow most calculated reactive intermediates to reach

144 steady state, but short enough to prevent the buildup of secondary products. An additional

145 lifetime of two days was assumed for some calculated long-lived species such as organic acids

146 and alcohols to avoid unexpected accumulation of these species in the model. At the end of 24

147 hours, the model generated time series of OH, HO_2, RO_2, and other reactive intermediates. The

148 box model covered the entire P-3B flight track during DISCOVER-AQ, including the eight

149 science sites where the P-3B conducted spirals. Note that unlike a three-dimensional chemical

150 transport model, the zero-dimensional box model simulations did not include advection and

151 emissions. Although advection and emissions are certainly important factors for the air pollution

152 formation, they can be omitted in the box model since all of the long-lived radical and O_3

153 precursors were measured and used to constrain the box model calculations. The box model

154 analysis is necessary for ozone production and its sensitivity to NO_x and VOCs because the box

155 model was constrained to measured species (e.g., NO, NO_2, CO, HCHO, etc.) and

156 meteorological parameters (e.g., photolysis frequencies) that are essential to calculate ozone

157 production rates. Even though there is good agreement in general between the box model and

158 the 3D model, there are still some differences between the measurements and the output from the

159 3D model that are shown below, e.g., NOx, CO, HCHO and photolysis frequencies.

160

161 **2.3 WRF-CMAQ Model Simulations**

162 The WRF model was run from 18 August 2013 to 1 October 2013 with nested domains

163 with horizontal resolutions of 36, 12, 4, and 1 km and 45 vertical levels. This work utilized

164 results from the 4 km domain. The modeling domains are shown in Figure 3. WRF was run

165 straight through (i.e., was not re-initialized at all) using an iterative technique developed at the

166 EPA and described in Appel et al. (2014). Observational and analysis nudging were performed

167 on all domains. Model output was saved hourly for the 36 and 12 km domains, every 20 minutes

168 for the 4 km domain, and every 5 minutes for the 1 km domain. WRF and CMAQ configuration

169 options and inputs are shown in Table 1.

170 WRF model results were used to drive the CMAQ model offline. The 2012 baseline

171 anthropogenic emissions from the Texas Commission on Environmental Quality (TCEQ) were

172 used as input to CMAQ. These emissions contain the most-up-to-date Texas anthropogenic

173 emissions inventory and a compilation of emissions estimates from Regional Planning Offices

174 throughout the US. Biogenic emissions were calculated online within CMAQ with Biogenic

175 Emission Inventory System (BEIS). Lightning emissions were also calculated online within

176 CMAQ. CMAQ was run with the process analysis tool to output ozone production rate ($P(O_3)$),

177 ozone loss rate ($L(O_3)$), and net ozone production rate (net $P(O_3)$) as well as ozone production

178 efficiency (OPE).

179

180 **3. RESULTS**

181 **3.1 Photochemical O_3 Production Rate, Sensitivity, and Diurnal Variations**

182 Figure 4 shows the net ozone production rate, net $P(O_3)$, calculated using the box model

183 results along the P-3B flight track for all flight days during the Houston deployment. There are

184 several $P(O_3)$ hotspots over the Houston Ship Channel located to the east/southeast of downtown

185 Houston as well as downwind, over Galveston Bay. This is expected because of large emissions

186 of NO_x and VOCs from the Houston Ship Channel, where the highest $P(O_3)$ was observed – up

187 to ~140 ppbv hr^{-1}. $P(O_3)$ values up to ~80-90 ppbv hr^{-1} were observed over Galveston Bay,

188 mainly on September 25, 2013, consistent with high ozone levels observed across the Houston

189 area on that day. Similar instantaneous ozone production rates have been observed in two

190 previous studies in Houston in 2000 and 2006 [Kleinman et al., 2002a; Mao et al., 2010].

191   Figure 5 shows the indicator L_N/Q of ozone production sensitivity along the P-3B flight

192 track for all flight days during the Houston deployment. $P(O_3)$ was mainly VOC-sensitive over

193 the Houston Ship Channel and its surrounding urban areas due to large NO_x emissions. Over

194 areas away from the center of the city with relatively low NO_x emissions, $P(O_3)$ was usually

195 NOx-sensitive. Vertical profiles of $P(O_3)$, $L(O_3)$, and net ozone production calculated using the

196 box model results (Figure 6) show that:

197 (1) $RO_2 + NO$ makes about the same amount of O_3 as $HO_2 + NO$ in the model;

198 (2) O_3 photolysis followed by $O(^1D)+H_2O$ is a dominant process for the photochemical ozone

199 loss;

200 (3) the maximum net $P(O_3)$ appeared near the surface below 1 km.

201   In the diurnal variations of $P(O_3)$, a broad peak in the morning with significant $P(O_3)$ in

202 the afternoon was obtained on ten flight days during DISCOVER-AQ in Houston (Figure 7).

203 High $P(O_3)$ mainly occurred with $L_N/Q > 0.5$ (i.e., in the VOC sensitive regime). The diurnal

204 variation of L_N/Q indicates that $P(O_3)$ was mainly VOC sensitive in the early morning and then

205 transitioned towards the NO_x sensitive regime later in the day (Figure 8). High $P(O_3)$ in the

206 morning was mainly associated with VOC sensitivity due to high NO_x levels in the morning

207 (points in the red circle in Figure 8). Although $P(O_3)$ was mainly NO_x sensitive in the afternoon

208 between 12:00 and 17:00 Central Standard Time, CST (UTC-6 hours), there were also periods

209 and locations when $P(O_3)$ was VOC sensitive, e.g., the points with $LN/Q > 0.5$ between 12:00

210 and 17:00 (CST) in Figure 8.

211   Diurnal variations of ozone production rate at eight individual locations where the P-3B

212 conducted vertical spirals show that the ozone production is greater than 10 ppb hr^{-1} on average

213 at locations with high NO_x and VOC emissions, such as Deer Park, Moody Tower and

214 Channelview, while at locations away from the urban center with lower emissions, such as

215 Galveston, Smith Point, and Conroe, the ozone production usually averaged less than 10 ppb hr^{-1}

216 (Figure 9). The dependence of $P(O_3)$ on the NO mixing ratio ([NO]) shows that when [NO] is

217   less than ~1 ppbv, ozone production increases as the [NO] increases, i.e., $P(O_3)$ is in NOx

218   sensitive regime. When the NO mixing ratio is greater than ~1 ppbv, ozone production levels off,

219   i.e., $P(O_3)$ is in a NOx saturated regime (Figure 10). It was also found that at a given NO mixing

220   ratio, a higher production rate of HO_x results in a higher ozone production rate. Diurnal

221   variations of the indicator of ozone production sensitivity to NO_x and VOCs, L_N/Q, at eight

222   individual locations where the P-3B conducted vertical spirals show that (1) at Deer Park, $P(O_3)$

223   was mostly VOC sensitive for the entire day; (2) at Moody Tower and Channelview, $P(O_3)$ was

224   VOC sensitive or in the transition regime; and (3) at Smith Point and Conroe, $P(O_3)$ was mostly

225   NOx sensitive for the entire day; and Galveston, West Houston, and Manvel Croix $P(O_3)$ was

226   VOC sensitive only in the early morning (Figure 11).

227

228   **3.2 Ozone Production Efficiency**

229   Ozone production efficiency (OPE) is defined as the number of molecules of oxidant Ox

230    $(= O_3 + NO_2)$ produced photochemically when a molecule of NO_x $(= NO + NO_2)$ is oxidized. It

231   conveys information about the conditions under which O_3 is formed and is an important

232   parameter to consider when evaluating impacts from NO_x emission sources [Kleinman et al.,

233   2002]. The OPE can be deduced from atmospheric observations as the slope of a graph of O_x

234   concentration versus the concentration of NO_x oxidation products. The latter quantity is denoted

235   as NO_z and is commonly measured as the difference between NO_y (sum of all odd-nitrogen

236   compounds) and NO_x, i.e. $NO_z = NO_y - NO_x$.

237   Figure 12 shows the photochemical oxidant O_x as a function of NO_z during DISCOVER-

238   AQ in Houston in 2013. The two data sets plotted here were collected on September 25 and 26,

239   when high ambient ozone concentrations were observed, and for the data collected during all

240   other flights. Note that the slopes obtained from these two data sets are essentially the same and

241   an average OPE of ~8 is derived from the observations, meaning that 8 molecules of ozone were

242   produced when one molecule of NO_x was consumed. Even though higher ozone concentrations

243   were observed on September 25 and 26, the OPE on these two days are not different from those

244   in other flights, indicating the ozone event on these two days was not caused by a higher OPE,

245   but mainly, by higher concentrations of ozone precursors (and thus higher ozone production rates)

246   and background ozone as indicated by the intercepts in the regression of the two data sets in

247   Figure 12**.** The high ozone observed on those days could also be due to slower ventilation and

different meteorological conditions such as a lower boundary layer height, northerly transport from inland air pollution source regions, stagnant conditions from the high-pressure system, and the bay and gulf breezes.

The OPE value of ~8 during DISCOVER-AQ in Houston in 2013 is greater than the average OPE value obtained during the Texas Air Quality Study in 2006 (TexAQS2006; OPE=5.9±1.2) [Neuman et al., 2009] and TexAQS2000 (OPE=5.4) [Ryerson et al., 2003]. One possible reason for this increased OPE is the continuous reduction in NO_x emissions in Houston from 2000 to 2013 pushed NO_x levels closer to 1 ppbv in 2013 (Figure S1), thus OPE increased since OPE increases as NO_x decreases when the NO_x level is greater than ~1 ppbv (Figure 13).

Houston area OPE values range from about a factor of 1.3 to 2 higher than the OPEs calculated from the DISCOVER-AQ 2011 study in Maryland, likely due to higher photochemical reactivity in Houston (Figure S4). The 2011 Maryland OPEs ranged from 3.4 to 6.1 when all measured data below 1 km are used (Ren, X., unpublished data). An OPE of ~8 was calculated [He et al., 2013] for the 2011 Maryland DISCOVER-AQ campaign for measured data below the 850 hPa level during vertical spirals with a strong linear correlation ($r^2 > 0.8$) between O_x and NO_z. Additionally, OPEs of 7.7-9.7 were obtained from a ground site during the New England Air Quality Study (NEAQS) 2002 (Griffin et al., 2004).

When calculating ozone production efficiency using observed O_x and NO_z, it is important to know whether there is substantial loss of nitric acid (HNO_3), because it can affect the OPE by reducing the NO_z [Trainer et al., 1993; 2000; Neuman et al., 2009] and thus bias the OPE high. The derived OPE in Figure 12 is only valid when there is minimum loss of NO_z (especially HNO_3) from the source region to the point of observations. Neuman et al. [2009] found that $\Delta CO/\Delta NOy$, i.e., the slope in a CO versus NO_y plot, is an indicator for distinguishing plumes with efficient O_3 formation from plumes with similarly high O_3 to NO_x oxidation products correlation slopes caused by variable mixing of aged polluted air depleted in HNO_3. A typical $\Delta CO/\Delta NO_y$ ranges from ~40 in background air to ~4-7 in fresh emission plumes in Houston [Neuman et al., 2009]. The $\Delta CO/\Delta NO_y$ was examined at different times of the day on September 25 and 26. The results indicate that the $\Delta CO/\Delta NO_y$ was about 6.2 (Figure 14a) throughout the day with variation between 6.0 and 7.0 (Figure 14). This demonstrates that the observed O_3 formation was from fresh plumes and was not caused by variable mixing of aged polluted air depleted in HNO_3.

279   Using both the box model and CMAQ model results, OPE can also be calculated

280   according to its definition, i.e., the net ozone formation rate divided by the formation rate of

281   NO_z. Net $P(O_3)$ was calculated using Eq. (1), while the NO_z formation rate is the sum of HNO_3

282   and organic nitrate formation rates. The agreement between the box model-derived and the

283   CMAQ-derived OPEs is very good, with the mean OPEs of 14.8±7.4 in the box model and

284   16.6±8.1 in the CMAQ model. The dependence of OPE on NO_x is also similar for both the box

285   and CMAQ models (Figure 13). On average, the maximum of OPE appears at a NO_x level

286   around 1 ppbv. In general, if the NO_x level is below 1 ppbv, OPE increases as the NO_x level

287   increases, while if the NO_x level is above 1 ppbv, OPE decreases as the NO_x level increases

288   (Figure 13).

289   The OPE values calculated using the CMAQ and box model are greater than the values

290   derived from the observations using the slope in the scatter plot of Ox versus NO_z in Figure 12.

291   This is expected because in the calculation of OPE using the box and CMAQ model results, a

292   few ozone loss processes, such as ozone dry deposition and horizontal/vertical dispersion, were

293   not considered. This could result in higher calculated ozone production rates using the model

294   results.

295   Spatial variations of OPE demonstrate that except for a few hotspots over Downtown

296   Houston and the Houston Ship Channel, most large OPEs appear away from the urban center,

297   e.g., the northwest and southeast of the area, while in areas with high NO_x emissions close to the

298   urban center lower OPEs were generally observed (Figure 15). This is again consistent with the

299   results in Figure 13 that the maximum of OPE appears at a NO_x level around 1 ppbv.

300

4. Discussion and Conclusions

302   On average, ozone production $P(O_3)$, was about 20-30 ppbv hr^{-1} in the morning and 5-10

303   ppbv hr^{-1} in the afternoon during DISCOVER-AQ in Houston in 2013. The diurnal variation of

304    $P(O_3)$ shows a broad peak in the morning with significant $P(O_3)$ in the afternoon obtained on ten

305   flight days in September 2013. High $P(O_3)$ mainly occurred with L_N/Q greater than 0.5, i.e., in

306   the VOC sensitive regime. Since $P(O_3)$ depends on NO_x levels and radical production rate, it

307   increases as [NO] increases up to ~1 ppbv and then levels off with further increases of [NO]. At

308   a given [NO], a higher production rate of HO_x results in a higher ozone production rate. This has

309   implications for the NO_x control strategies in order to achieve the ozone control goal.

10

310   The DISCOVER-AQ campaign in Houston is unique because of its large spatial coverage
311   and thus spatial variations of ozone production and its sensitivity to NOx and VOCs. Diurnal
312   variations of $P(O_3)$ at eight individual locations where the P-3B conducted vertical spirals show
313   that the $P(O_3)$ is on average more than 10 ppbv hr^{-1} at locations with high NO_x and VOC
314   emissions, such as Deer Park, Moody Tower, and Channelview, while at locations away from the
315   urban center with lower emissions of ozone precursors such as Galveston, Smith Point, and
316   Conroe, the ozone production rate is usually less than 10 ppbv hr^{-1} on average. Hotspots of $P(O_3)$
317   were observed over Downtown Houston and the Houston Ship Channel due to significant
318   emissions in these areas.

319   Ozone production tended more towards VOC sensitive in the morning with high $P(O_3)$
320   and in general, NO_x sensitive in the afternoon with some exceptions. It was found that during
321   some afternoon time periods and locations, $P(O_3)$ was VOC sensitive. The diurnal variation of
322   L_N/Q indicates that $P(O_3)$ was mainly VOC sensitive in the early morning and then transitioned
323   towards the NO_x sensitive regime later in the day. High $P(O_3)$ in the morning was mainly
324   associated with VOC sensitivity due to high NO_x levels in the morning. Specifically, Deer Park
325   was mostly VOC sensitive for the entire day, Moody Tower and Channelview were VOC
326   sensitive or in the transition regime, and Smith Point and Conroe were mostly NO_x sensitive for
327   the entire day.

328   Based on the measurements on the P-3B, ozone production efficiency (OPE) was about 8
329   during DISCOVER-AQ 2013 in Houston. This OPE value is greater than the average OPE value
330   (5.9 ± 1.2) obtained during the Texas Air Quality Study in 2006 (TexAQS2006), likely due to the
331   reduction in NO_x emissions in Houston between 2006 and 2013 that pushed NO_x levels closer to
332   1 ppbv in 2013 from higher NOx levels in previous years. The results from this work strengthen
333   our understanding of O_3 production; they indicate that controlling NO_x emissions will provide air
334   quality benefits over the greater Houston metropolitan area in the long run, but in selected areas
335   controlling VOC emissions will also be beneficial.

336

References

Appel, K.W., Gilliam, R.C., Pleim, J.E., Pouliot, G.A., Wong, D.C., Hogrefe, C., Roselle, S.J., and Mathur, R.: Improvements to the WRF-CMAQ modeling system for fine-scale air quality simulations, EM, 16-21 2014.

Canty, T. P., Hembeck, L., Vinciguerra, T. P. , Anderson, D. C. , Goldberg, D. L. , Carpenter, S. F. , Allen, D. J. , Loughner, C. P. , Salawitch, R. J. , and Dickerson, R. R.: Ozone and NOx chemistry in the eastern US: evaluation of CMAQ/CB05 with satellite (OMI) data, *Atmospheric Chemistry and Physics*, *15*(19), 10965-10982, doi:10.5194/acp-15-10965-2015, 2015.

Chen, S., Ren, X., Mao J., Chen, Z., Brune, W. H., Lefer, B., Rappenglück, B., Flynn J., Olson, J., Crawford, J. H.: A comparison of chemical mechanisms based on TRAMP–2006 field data, Atmos. Environ., 44(33), 4116-4125, 2010.

DISCOVER-AQ whitepaper, http://discover-aq.larc.nasa.gov/pdf/DISCOVER-AQ_science.pdf.

Finlayson-Pitts, B. J., and Pitts, J.: Chemistry of the upper and lower atmosphere: Theory, experiments and applications, Academic Press, San Diego, California, p.264-276, 2000.

Goldberg, D. L., Vinciguerra, T. P., Anderson, D. C., Hembeck, L., Canty, T. P., Salawitch, R. J., and Dickerson, R. R. CAMx Ozone Source Attribution in the Eastern United States using Guidance from Observations during DISCOVER-AQ Maryland, *Geophysical Research Letters*, doi: 10.1002/2015GL067332, 2016.

Griffin, R. J., Johnson, C. A., Talbot, R. W., Mao, H., Russo, R. S., Zhou, Y., and Sive B. C.: Quantification of ozoneformation metrics at Thompson Farm during the New England Air Quality Study (NEAQS) 2002, J. Geophys. Res., 109, D24302,doi:10.1029/2004JD005344, 2004.

He, H., Hembeck, L., Hosley, K. M., Canty, T. P., Salawitch, R. J., and Dickerson, R. R.: High

372   ozone concentrations on hot days: The role of electric power demand and NOx emissions,

373   Geophys. Res. Lett., 40, 5291–5294, doi:10.1002/grl.50967, 2013.

374

375   Jacob, D. J.: Introduction to Atmospheric Chemistry, Princeton University Press, New Jersey,

376   1999.

377   Kleinman, L. I., Daum, P. H., Lee, Y.-N, Nunnermacker, L. J., Springston, S. R., Weinstein-

378   Lloyd J., and Rudolph, J.: Sensitivity of ozone production rate to ozone precursors. Geophys.

379   Res. Lett., 28, 2903–2906 , doi: 10.1029/2000GL012597, 2001.

380   Kleinman, L. I., Daum, P. H., Lee, Y.-N., Nunnermacker, L. J., Springston, S. R., Weinstein-

381   Lloyd, J., and Rudolph, J.: Ozone production efficiency in an urban area, J. Geophys. Res.,

382   107 (D23), 4733, doi:10.1029/2002JD002529, 2002.

383   Kleinman, L. I., Daum, P. H., Lee, Y.-N., Nunnermacker, L. J., Springston, S. R., Weinstein-

384   Lloyd, J., and Rudolph, J.: A comparative study of ozone production in five U.S.

385   metropolitan areas, J. Geophys. Res., 110, D02301, doi:10.1029/2004JD005096, 2005a.

386   Kleinman, L. I.: The dependence of tropospheric ozone production rate on ozone precursors,

387   Atmos. Environ., 39(3), 575–586, doi:10.1016/j.atmosenv.2004.08.047, 2005b.

388   Lei, W., Zhang, R., Tie, X., and Hess, P.: Chemical characterization of ozone formation in the

389   Houston-Galveston area: A chemical transport model study, J. Geophys. Res., 109, D12301,

390   doi:10.1029/2003JD004219, 2004.

391   Li, G., Zhang, R., Fan, J., and Tie, X.: Impacts of biogenic emissions on photochemical ozone

392   production in Houston, Texas, J. Geophys. Res., 112, D10309, doi:10.1029/2006JD007924,

393   2007.

394   Mallet, V. and Sportisse, B.: A comprehensive study of ozone sensitivity with respect to

395   emissions over Europe with a chemistry-transport model, J. Geophys. Res., 110, D22302,

396   doi:10.1029/2005JD006234, 2005.

397   Mao, J., Ren, X., Chen, S., Brune, W. H., Chen, Z., Martinez, M., Harder, H., Lefer, B.,

398   Rappenglück, B., Flynn, J., and Leuchner, M.: Atmospheric oxidation capacity in the

399   summer of Houston 2006: Comparison with summer measurements in other metropolitan

400   studies, Atmos. Environ., 44(33), 4107-4115, 2010

401   Molina, M. J., and Molina, L. T.: Megacities and atmospheric pollution, J. Air Waste Manage.,

402   54, 644–680, 2004.

403   Neuman, J. A., et al.: Relationship between photochemical ozone production and NOx oxidation

404   in Houston, Texas, J. Geophys. Res., 114, D00F08, doi:10.1029/2008JD011688, 2009.

405   Ren, X., van Duin, D., Cazorla, M., Chen, S., Mao, J., Zhang, L., Brune, W. H., Flynn, J. H.,

406   Grossberg, N., Lefer, B. L., Rappenglück, B., Wong, K. W., Tsai, C., Stutz, J., Dibb, J. E.,

407   Jobson, B. T., Luke, W. T., and Kelley, P.: Atmospheric oxidation chemistry and ozone

408   production: Results from SHARP 2009 in Houston, Texas, J. Geophys. Res., 118, 5770–5780,

409   2013.

410   Ryerson, T. B., et al., Effect of petrochemical industrial emissions of reactive alkenes and NOx

411   on tropospheric ozoneformation in Houston, Texas, J. Geophys. Res., 108(D8), 4249,

412   doi:10.1029/2002JD003070, 2003.

413   Sillman, S.: The use of NO_y, H_2O_2, and HNO_3 as indicators for O_3-NO_x-hydrocarbon sensitivity

414   in urban locations, J. Geophys. Res., 100, 14,175–14,188, 1995.

415   Sillman, S., Vautard, R., Menut, L., and Kley, D.: O_3-NO_x-VOC sensitivity and NO_x-VOC

416   indicators in Paris: Results from models and Atmospheric Pollution Over the Paris Area

417   (ESQUIF) measurements, J. Geophys. Res., 108(D17), 8563, doi:10.1029/2002JD001561,

418   2003.

419   Tang, X., Wang, Z., Zhu, J., Gbaguidi, A. E., Wu, Q., Li, J., and Zhu, T., Sensitivity of ozone to

420   precursor emissions in urban Beijing with a Monte Carlo scheme. Atmos. Environ., 44, 3833-

421   3842, 2010.

422   Thielmann, A., Pre´voˆt, A. S. H., and Staehelin, J.: Sensitivity of ozone production derived

423   from field measurements in theItalian Po basin, J. Geophys. Res., 107(D22), 8194,

424   doi:10.1029/2000JD000119, 2002.

425   Trainer, M., et al.: Correlation of ozone with NOy in photochemically aged air, J. Geophys. Res.,

426   98, 2917 – 2925, doi:10.1029/ 92JD01910, 1993.

427   Trainer, M., Parrish, D. D., Goldan, P. D., Roberts, J., and Fehsenfeld, F. C.: Review of

428   observation-based analysis of the regional factors influencing ozone concentrations, Atmos.

429   Environ., 34, 2045 – 2061, doi:10.1016/S1352-2310(99)00459-8, 2000.

430   Xue, L. K., Wang, T., Gao, J., Ding, A. J., Zhou, X. H., Blake, D. R., Wang, X. F., Saunders, S.

431   M., Fan, S. J., Zuo, H. C., Zhang, Q. Z., and Wang, W. X.: Ozone production in four major

432   cities of China: sensitivity to ozone precursors and heterogeneous processes, Atmos. Chem.

433   Phys. Discuss., 13, 27,243–27,285, doi:10.5194/acpd-13-27243-2013, 2013.

434 Yarwood, G., Rao, S., Yocke, M., and Whitten, G. Z.: Updates to the Carbon Bond Mechanism:

435   CB05, Final Report to the US EPA (RT-0400675),(http://www.camx.com/publ/

436   pdfs/CB05_Final_Report_120805.pdf), 2005.

437 Zaveri, R. A., Berkowitz, C. M., Kleinman, L. I., Springston, S. R., Doskey, P. V., Lonneman, W.

438   A., and Spicer, C. W.: Ozone production efficiency and NOx depletion in an urban plume:

439   Interpretation of field observations and implications for evaluating O3-NOx-VOC

440   sensitivity, J. Geophys. Res., 108(D14), 4436, doi:10.1029/2002JD003144, 2003.

441

442

Table 1. WRF and CMAQ model options that were used in both the original and improved
modeling scenarios.

Weather Research and Forecasting (WRF) Version 3.6.1 Model Options	
Radiation	Long Wave: Rapid Radiative Transfer Model (RRTM)
	Short Wave: Goddard
Surface Layer	Pleim-Xiu
Land Surface Model	Pleim-Xiu
Boundary Layer	Asymmetric Convective Model (ACM2)
Cumulus	Kain-Fritsch
Microphysics	WRF Single-Moment 6 (WSM-6)
Nudging	Observational and analysis nudging
Damping	Vertical velocity and gravity waves damped at top of modeling domain
SSTs	Multi-scale Ultra-high Resolution (MUR) SST analysis (~1 km resolution)
Meteorological Initial and Boundary Conditions and Analysis Nudging Inputs	NAM 12 km
Observational Nudging Inputs	NCEP ADP Global Surface and Upper Air Observational Weather Data
CMAQ Version 5.0.2 Model Options	
Chemical Mechanism	Carbon Bond (CB05)
Aerosol Module	Aerosols with aqueous extensions version 5 (AE5)
Dry deposition	M3DRY
Vertical diffusion	Asymmetric Convective Model 2 (ACM2)
Emissions	2012 TCEQ anthropogenic emissions Biogenic Emission Inventory System (BEIS) calculated within CMAQ
Chemical Initial and Boundary Conditions	Model for OZone and Related chemical Tracers (MOZART) Chemical Transport Model (CTM)

445

446 **Figures:**

net P(O$_3$) (ppb/hr)
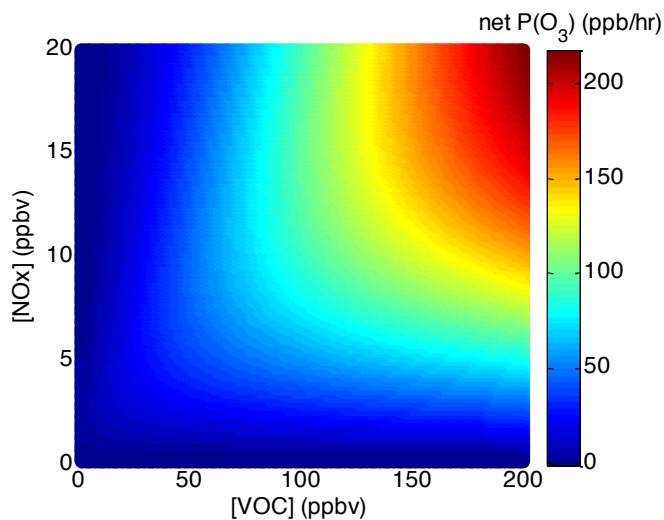
447

448 **Figure 1.** Ozone production empirical kinetic modeling approach (EKMA) diagram using a box

449 model results with NOx levels varying from 0-20 ppbv and VOC levels from 0-200 ppbv while

450 the mean concentrations of other species and the speciation of NOx and VOCs observed during

451 DISCOVER-AQ in Houston in 2013 were used to constrain the box model. This diagram clearly

452 shows the sensitivity of ozone production to NO$_x$ and VOCs in Houston.

453

454
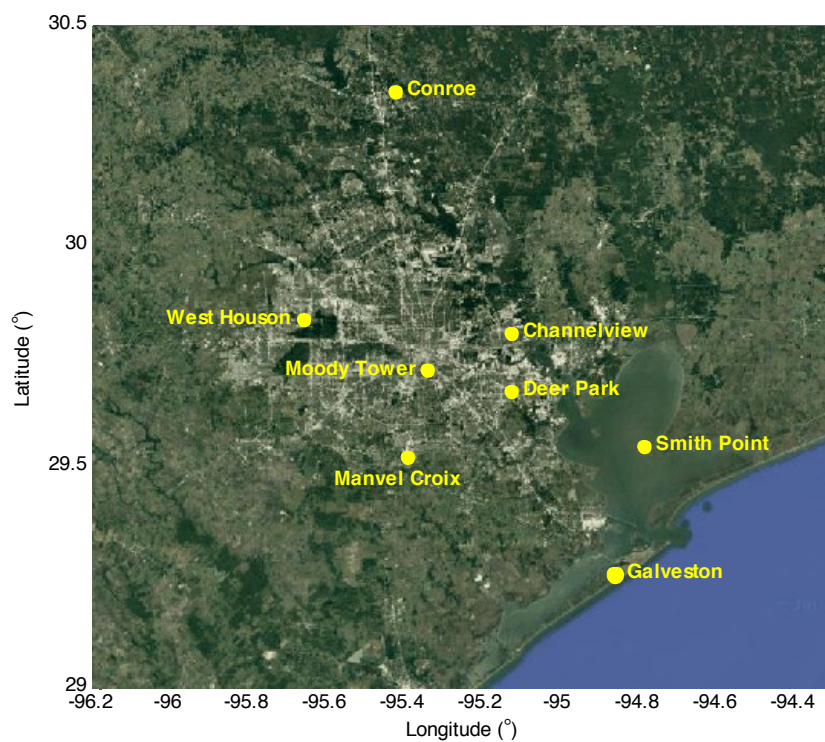
Figure 2. DISCOVER-AQ ground and spiral sites (yellow dots) during the September 2013
Houston campaign.

457

458

459
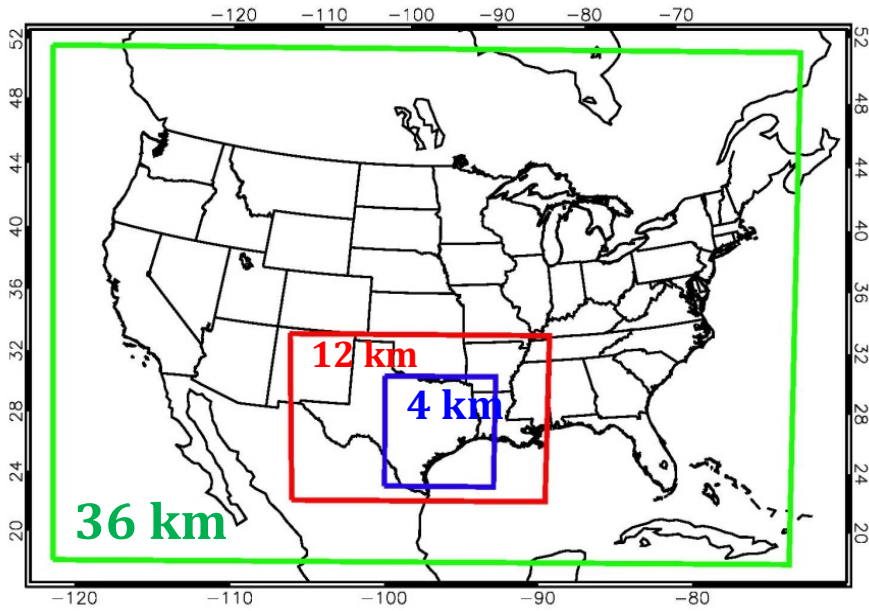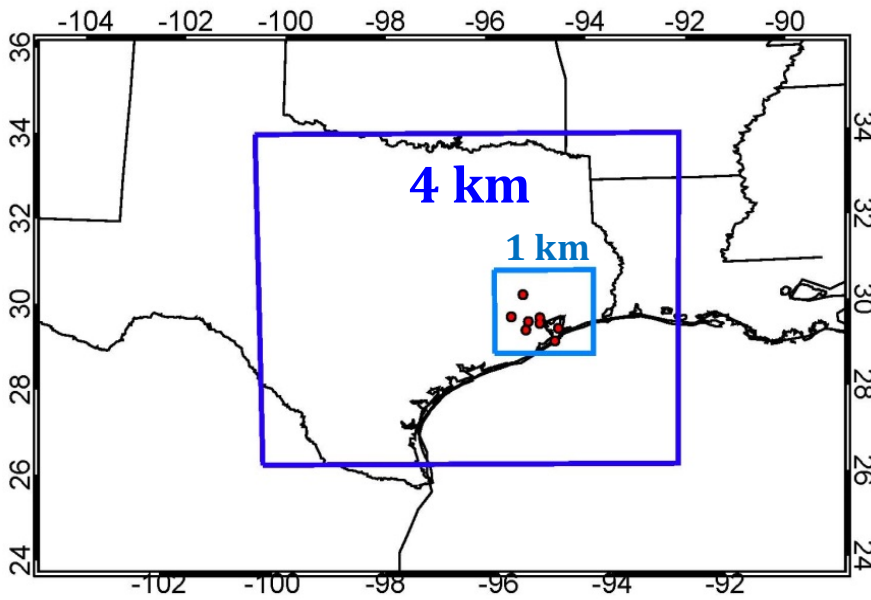
Figure 3. 36, 12, and 4 km CMAQ modeling domains (top); 4 and 1 km CMAQ modeling

domains. The red dots show the NASA P-3B aircraft spiral locations (bottom).

462

463

464

465
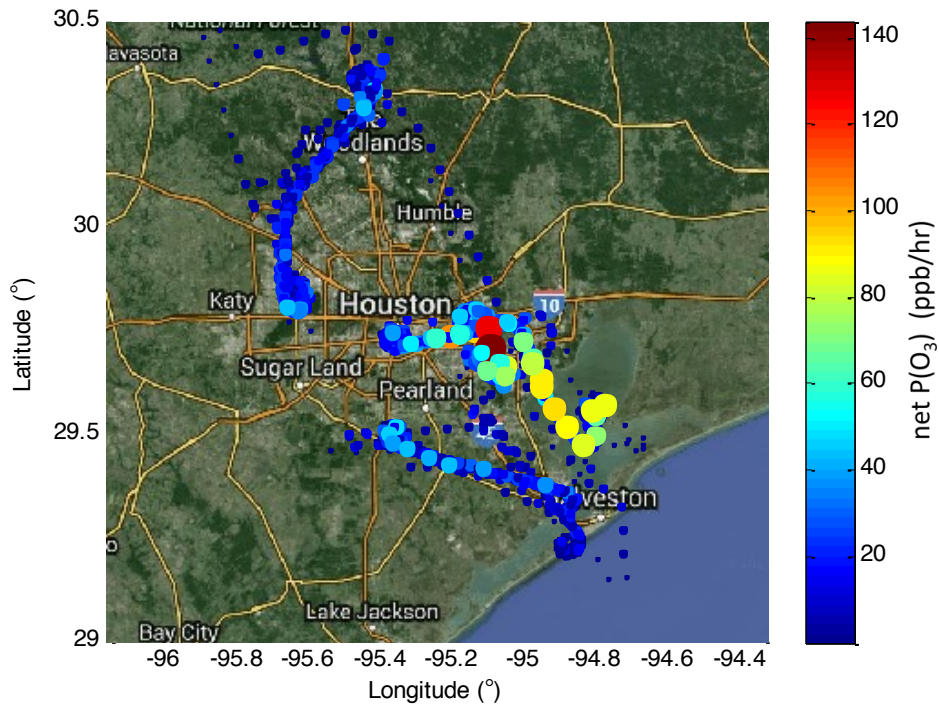
Figure 4. Net ozone production rate, net $P(O_3)$ calculated using the box model results along the P-3B flight track during DISCOVER-AQ in Houston in 2013. The size of dots is proportional to $P(O_3)$.

466

467

468

469

470
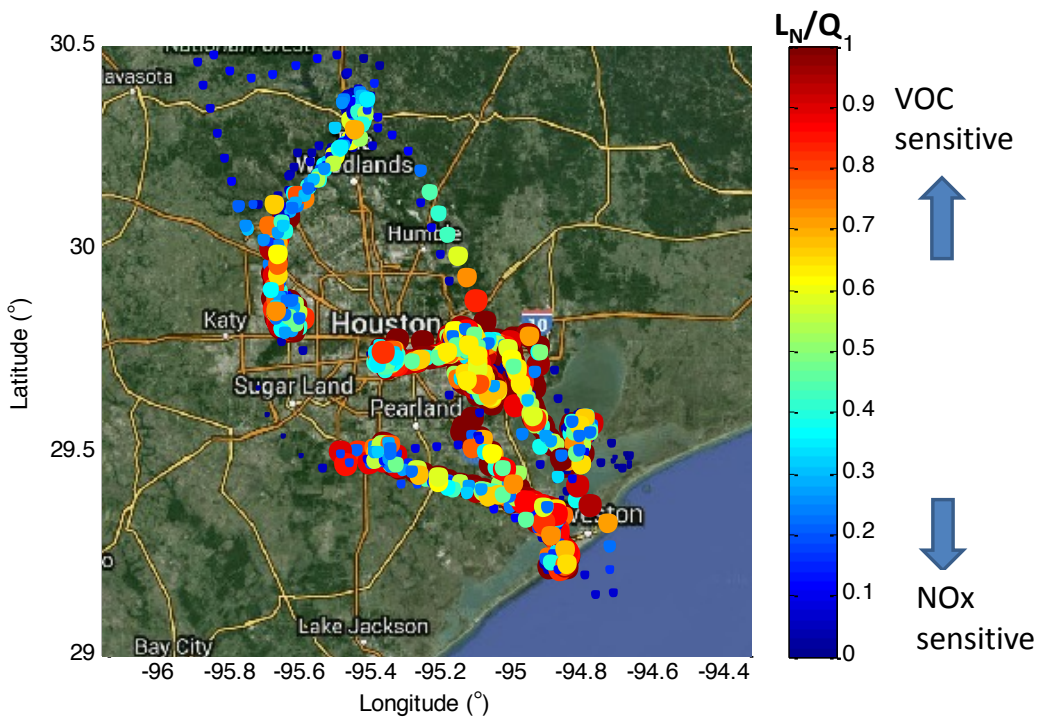
Figure 5. Ozone production sensitivity indicator, L_N/Q, along the P-3B flight track during DISCOVER-AQ in Houston in 2013. $P(O_3)$ is VOC-sensitive when $L_N/Q > 0.5$, and NOx-sensitive when $L_N/Q < 0.5$.

474
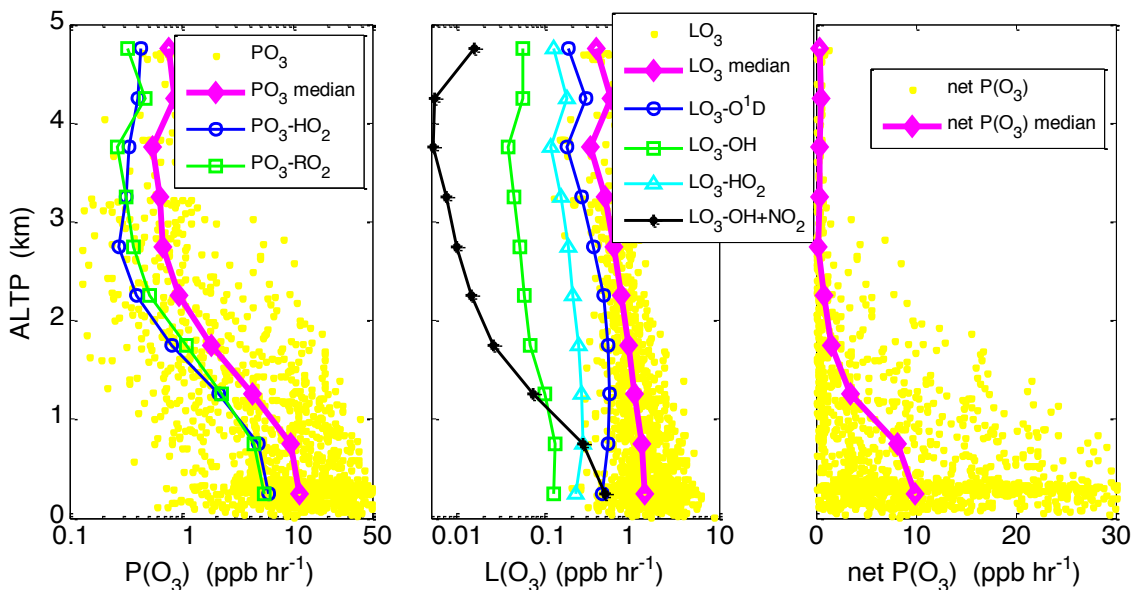
Figure 6. Vertical profiles of ozone production rate (left), ozone loss rate (middle), and net ozone production rate (right) during DISCOVER-AQ in Houston in 2013.

477
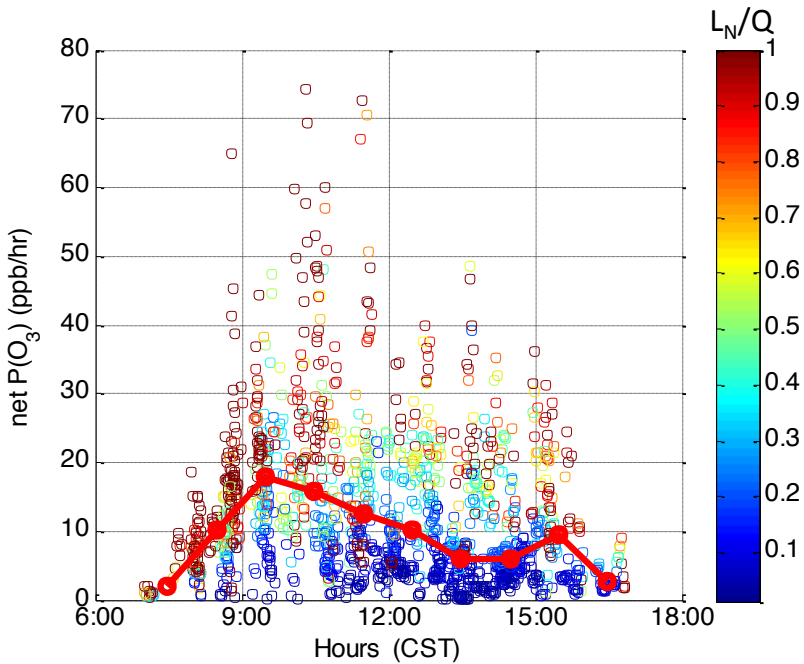
Figure 7. Diurnal variation of ozone production rate colored with the indicator L_N/Q on ten flight days during DISCOVER-AQ in Houston in 2013. The solid red circles represent the median values in hourly bins of $P(O_3)$. Data are limited with the pressure altitude less than 1000 m to represent the lowest layer of the atmosphere.


482
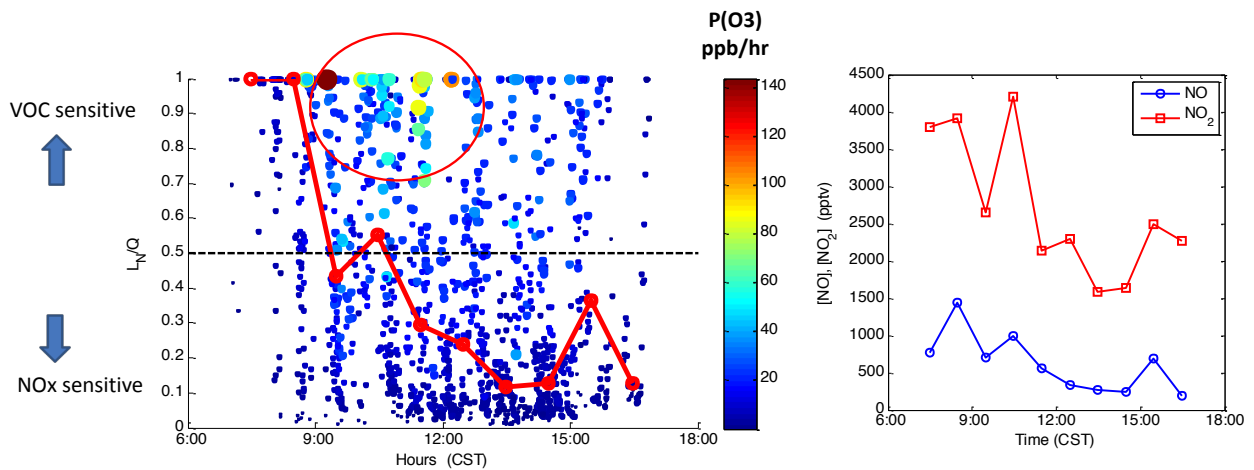
Figure 8. Diurnal variations of the indicator L_N/Q of ozone production rate sensitivity colored with ozone production rate and median hourly bins of L_N/Q shown in solid red circles (left) and median hourly NO and NO_2 concentrations (right) below 1000 m during DISCOVER-AQ in Houston in 2013.

22

487
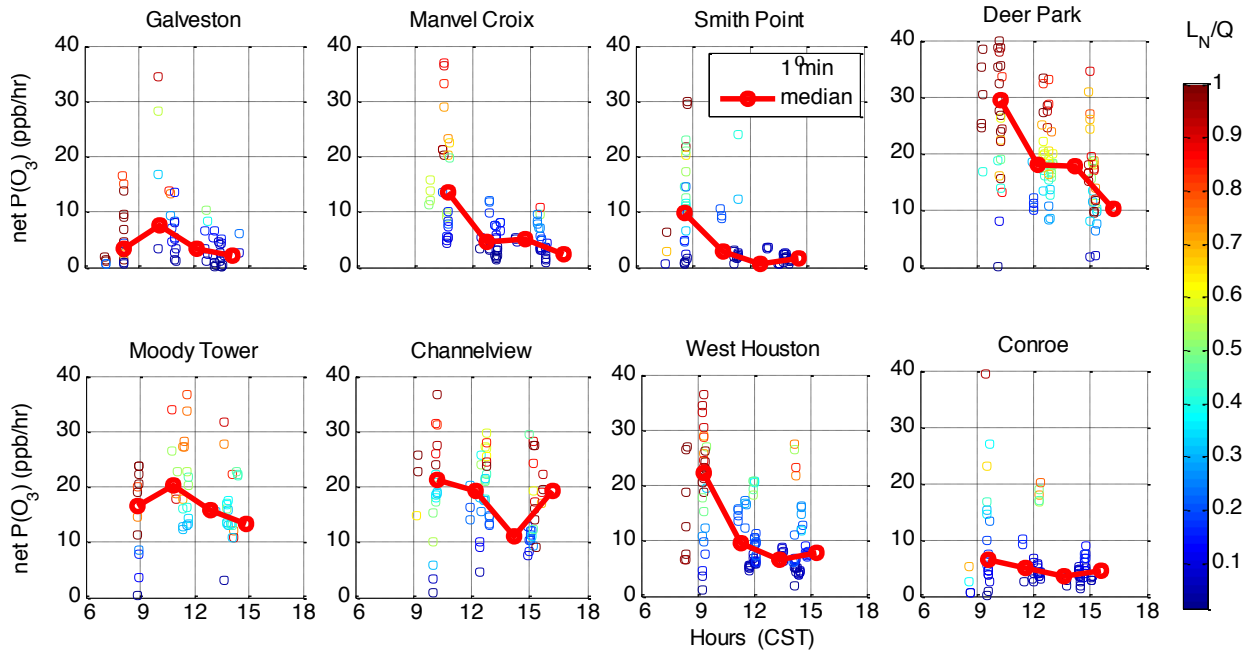
Figure 9. Diurnal variations of ozone production rate at eight individual spiral locations. Individual points are 1-min data colored with L_N/Q and the linked red circles represent the median values in hourly bins of $P(O_3)$. Data are limited with the pressure altitude less than 1000 m to represent the lowest layer of the atmosphere.

492

493

494
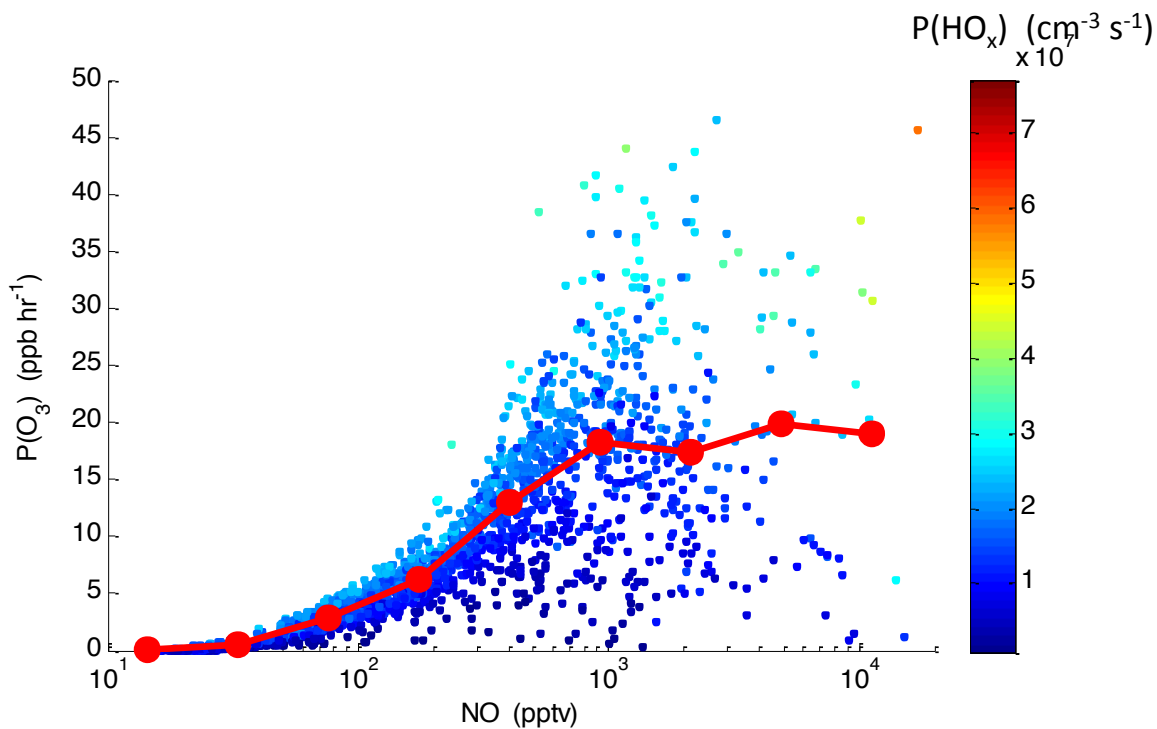
Figure 10. Ozone production as a function of NO mixing ratio. Individual data points are the 1-minute averages and are colored with the production rate of HOx (= OH + HO$_2$) during DISCOVER-AQ in Houston in 2013. The linked solid red circles represent the median values in [NO] bins. Note a log scale is used for the x-axis.

499

500

501
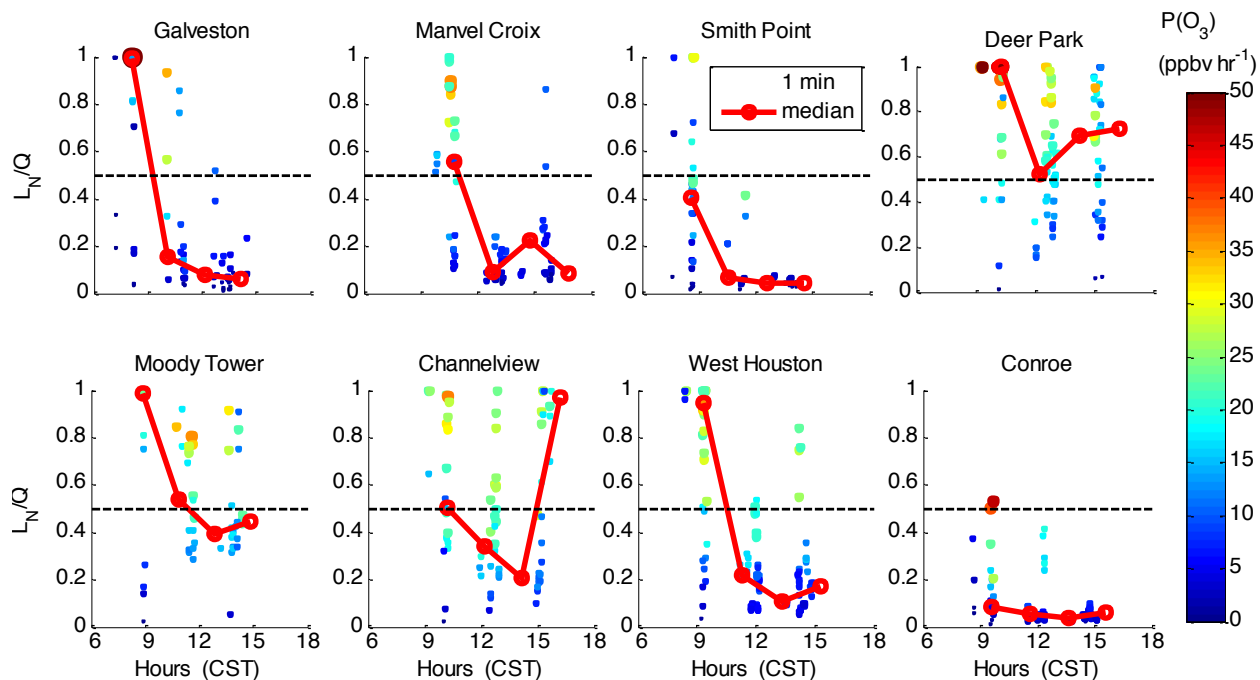
Figure 11. Diurnal variations of the indicator of ozone production sensitivity to NOx and VOCs, L_N/Q, at eight individual spiral locations during DISCOVER-AQ in Houston in 2013. Individual points are 1-min data colored by $P(O_3)$ and the linked red circles represent the median values in hourly bins of $P(O_3)$. Data are limited with the pressure altitude less than 1000 m to represent the lowest layer of the atmosphere.
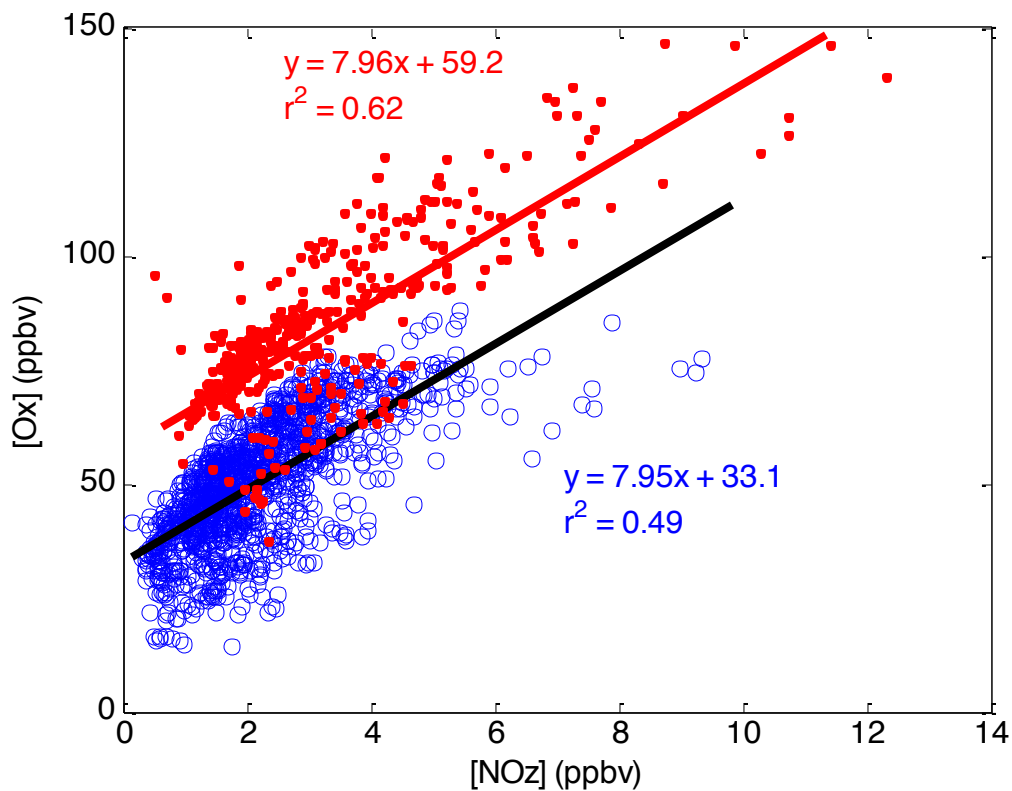
Figure 12. Photochemical oxidant, Ox ($=O_3+NO_2$) as a function of NOz ($=NOy-NOx$) during DISCOVER-AQ in Houston in 2013. Red dots are the data collected on September 25 and 26, 2013 when high ambient ozone concentrations were observed. Blue circles are the data collected during other flights. Data are limited with the pressure altitude less than 1000 m to represent the lowest layer of the atmosphere.
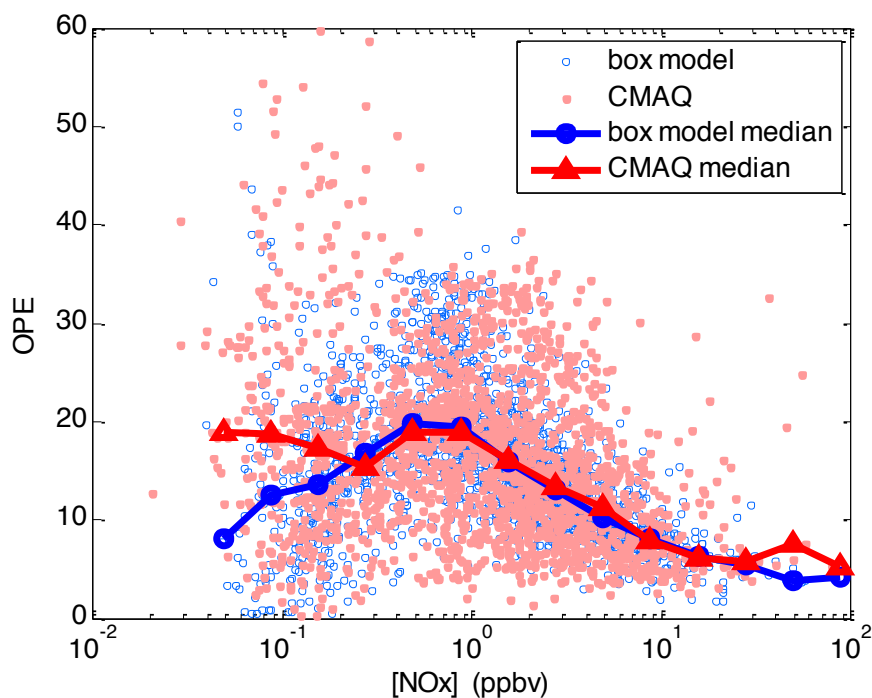
507

508

509

510

511

512

513

514

515

516

517

Figure 13. Ozone production efficiency (OPE) versus NOx in the box model (blue circles) and CMAQ model (pink dots) results. The linked blue circles show the median OPE values binned by NOx concentration in the box model, while the linked red triangles show the median OPE values binned by NOx concentration in the CMAQ model, OPE is calculated according to its definition as the net ozone formation rate divided by of the formation rate of NOz.
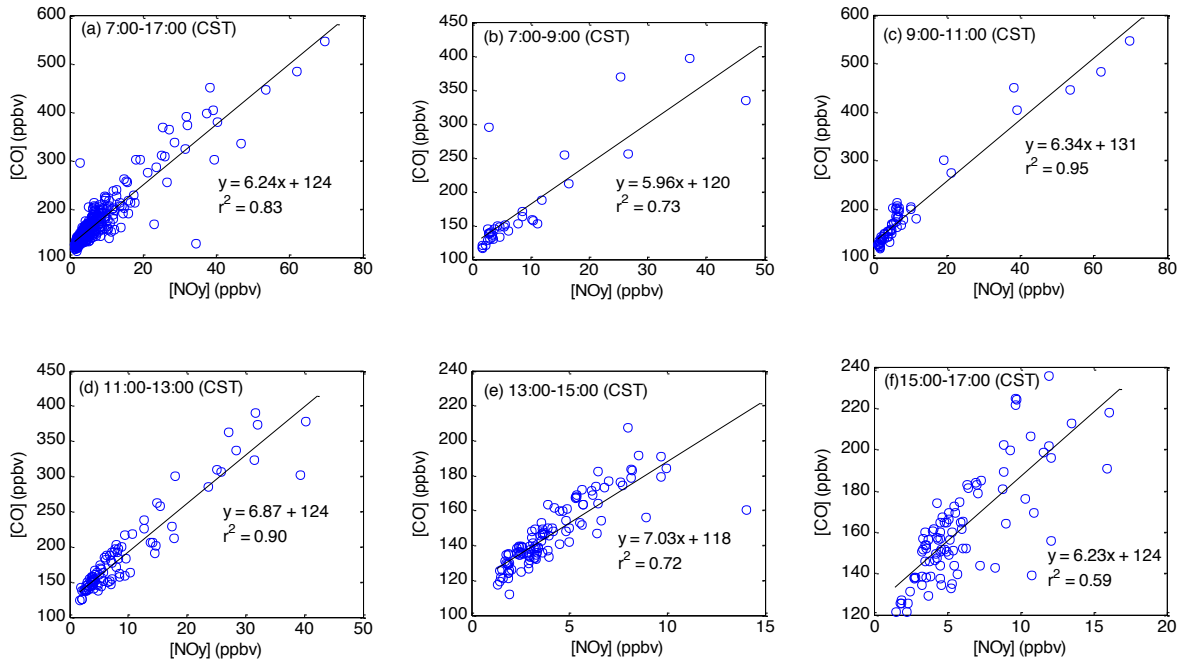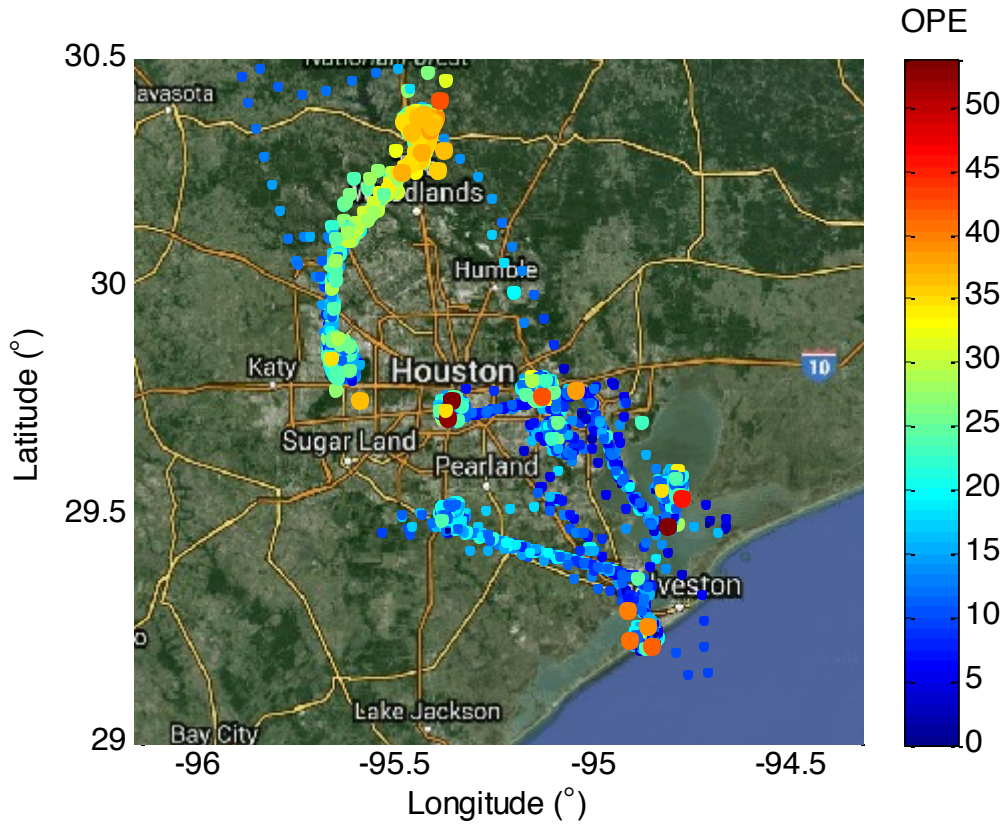
529

530

Figure 14. CO versus NOy and linear regression on September 25 and 26 at different times of the day: (a) 07:00-17:00 (all data), (b) 07:00-09:00, (c) 09:00-11:00, (d) 11:00-13:00, (e) 13:00-15:00, and (f) 15:00-17:00 (CST).

534

535

Figure 15. Ozone production efficiency (OPE) along the P-3B flight track during DISCOVER-AQ in Houston in 2013. OPE was calculated using the box model results as the ratio of net ozone formation rate to the formation rate of NOz.

539

540